Ultra-Wideband and Wide-Angle Insensitive Absorber Based on TCDA-Under-Tightly Coupled Dipole Array

Seongjung Kim and Sangwook Nam, *Senior Member, IEEE*

***Abstract*— In this article, an ultra-wideband and wide-angle insensitive absorber is proposed. The unit cell of the proposed structure consists of a tightly coupled dipole array (TCDA2) under another TCDA (TCDA1) that is twice the height of TCDA2 (TCDA-under-TCDA structure). TCDA1 of the unit cell acts as either a lossless (or lossy) antenna when the frequency is out of (or in) the operating frequency range of TCDA2. Reciprocity is applied to design TCDA1 as an absorber when the frequency is out of the operating frequency range of TCDA2 (lossless antenna region). On the other hand, the multisection impedance matching technique is applied for TCDA1 to be an absorber when the frequency is in the operating region of TCDA2 (lossy antenna region and reciprocity cannot be applied). In addition, a metasurface (MS) and vertical metal strip (VMS) are employed to develop the wide-angle insensitivity absorber. A −10 dB reflection bandwidth of 0.63–6.55 (10.4:1) is achieved with a 0.126λ_{low} at the lowest operating frequency under normal incidence. The bandwidth is moderately reduced to 0.69–6.75 (9.78:1) with a 0.138λ_{low} for the TE mode and 0.75–6.22 (8.29:1) with a 0.150λ_{low} for the TM mode under 45° oblique incidence. The measured results of the fabricated absorber using the transverse electromagnetic (TEM) cell are in good agreement with the simulated results.**

***Index Terms*— Absorber, dual polarization, low-profile, tightly coupled dipole array (TCDA), ultra-wideband, wide-angle insensitivity.**

I. Introduction

WITH the advancement of radar technologies [1], [2], several methodologies have been proposed to prevent the generation of electromagnetic (EM) waves. One such methodology is the use of an absorber to absorb incident EM waves [3], [4]. Traditionally, the Salisbury screen in which a homogeneous resistive sheet is located a quarter wavelength above the ground plane is used as an absorber [5]. Since the operating principle strongly depends on the electrical length between the resistive sheet and the ground plane, the bandwidth is inevitably narrow. To widen the bandwidth, Jauman introduced multilayer homogeneous resistive sheets at the expense of the profile [6]. However, to satisfy the increasing demands for widening the bandwidth of low-profile absorbers, it is necessary to determine the theoretical performance limit of their bandwidth and thickness characteristics. Rozanov and Konstantin [7] calculated the limit of the bandwidth given the thickness of the metal-backed absorber and determined that the thickness and absorption bandwidth share a mutual trade-off relationship.

To realize the ultimate performances of these absorbers, several studies have been conducted. The performance of a planar absorber is improved when the homogeneous resistive sheet is replaced by a periodic resistive frequency selective surface (FSS) [8], [9]. Absorbers with resistive FSS techniques, such as circuit analog absorbers (CAAs) [10], [11] and capacitive circuit absorbers (CCAs) [12], [13], have been previously studied. The CAAs have several merits such as low-profile, lightweight, and low-cost; furthermore, they can be easily fabricated. However, owing to the *RLC* resonators used in them, unwanted harmonic resonances are observed; therefore, they do not easily achieve ultra-wideband characteristics. To avoid harmonic resonances, the application of a low-pass *RC* circuit in absorbers, such as a CCA, is proposed, significantly improving the bandwidth. This improvement is vital for an ultra-wideband absorber. For example, the simulated profile of the CCA in [12] almost reached the theoretical limit.

For the absorber's design, a method based on antennas in a two-port network was proposed using the reciprocity theorem [14]. In this method, near-lossless antennas used as radiating devices can be adopted as absorbers because $S_{11} = S_{22}$, where 1 is the antenna port, whereas 2 is the Floquet port (FP) in the unit cell. A tightly coupled dipole array (TCDA) is a low-profile and wideband array antenna [15] employed as an absorber in [16] and [17]. In the existing studies conducted on TCDAs, considerable effort has been invested to lower their profile and widen their bandwidth and scan range [18]–[22]. However, ultra-wideband TCDAs, as reported in [18] and [19], cannot be directly used as an absorber by means of reciprocity since the loss of the antenna is not negligible (radiation efficiency > 73%), as reported in [18], and the polarization-rotated reflected wave by the polarization converter (PC) can be seen as a loss to the original polarization, as reported in [19].

Manuscript received July 25, 2020; revised January 12, 2021; accepted February 12, 2021. Date of publication March 1, 2021; date of current version September 3, 2021. This work was supported by the Institute of Information and Communications Technology Planning and Evaluation (IITP) grant funded by the Korea Government (MSIT) (Millimeter-Wave Metasurface-Based Dual-Band Beamforming Antenna-on-Package Technology for 5G Smartphone) under Grant 2020-0-00858. *(Corresponding author: Sangwook Nam.)*

The authors are with the Institute of New Media Communication (INMC), School of Electrical and Computer Engineering, Seoul National University, Seoul 08826, South Korea (e-mail: sjkim@ael.snu.ac.kr; snam@snu.ac.kr).

Color versions of one or more figures in this article are available at https://doi.org/10.1109/TAP.2021.3061008.

Digital Object Identifier 10.1109/TAP.2021.3061008

In previous studies on CAAs-, CCAs-, and TCDA-based absorbers, the wide-angle insensitivity was not remarkable; furthermore, the absorption rate deteriorated, particularly in the low-frequency bands, with an increase in the incidence angle. For example, the incidence angle is strictly limited to 30° owing to the degradation of the absorption rate [11]. The lowest operating frequency for an incidence angle of 45° in [16] was two times higher than that at 0°. Several studies focused on the profile and bandwidth for the Rozanov limit. However, for the absorber to suit several applications, the characteristic of wide-angle insensitivity is also essential. Thus, although several studies related to the subject were conducted, the bandwidths obtained for the absorbers are still narrower than desired [23]–[25]. Therefore, this study aims to realize an ultra-wideband, low-profile, and wide-angle insensitive absorber. The TCDA-under-TCDA structure is proposed to achieve ultra-wideband and low-profile characteristics. The reciprocity is applied when TCDA2 is in OFF-state, whereas the multilayer impedance transformer for matching plays a significant role when TCDA2 is in the ON state. In addition, we employ several techniques to achieve wide-angle insensitivity for wide bandwidth [22], [26].

The rest of the article is organized as follows. We present the design procedure, the equivalent circuit, and analysis of the proposed unit element in Section II. The experimental results obtained using the proposed 1-D array absorber and transverse EM (TEM) cell are discussed in Section III. Finally, the current study results are compared with those of existing state-of-the-art studies. The conclusions of the study are summarized in Section IV.

II. Design of the Proposed TCDA-Under-TCDA-Based Absorber

A. Brief Description of the Operating Principle of the Proposed Absorber and Equivalent Circuit

Fig. 1(a) shows the proposed basic unit structure. The operating principle can be described depending on the bands as shown in Fig. 1(f). In band1 ($0 - f_1$), the dipole in TCDA2 can be regarded as an open circuit since the frequency is too low compared with its operating frequency. Therefore, the proposed structure can be thought of as an absorber consisting of TCDA1 only. In band2 ($f_1 - f_2$), TCDA2 is operating as an absorber by itself. Thus, TCDA1 is considered equivalently to be in the free space since the downward wave from TCDA1 is absorbed by TCDA2. In band3 (f_2 ∼), the dipole in TCDA2 can be modeled as a highly reactive element since the frequency is above its resonant frequency. As a result, TCDA1 is located above a highly reactive surface (RS), behaving as an absorber, based again on reciprocity.

Fig. 2(a)–(c) shows the equivalent circuits of the proposed structure based on the operating principle explained above. In Fig. 2(d), the reflection characteristics of the equivalent circuits are compared with the simulation result of Fig. 1(a)–(c) structure. The results agree reasonably well and show that the explanation of the operation mechanism described above is accurate.

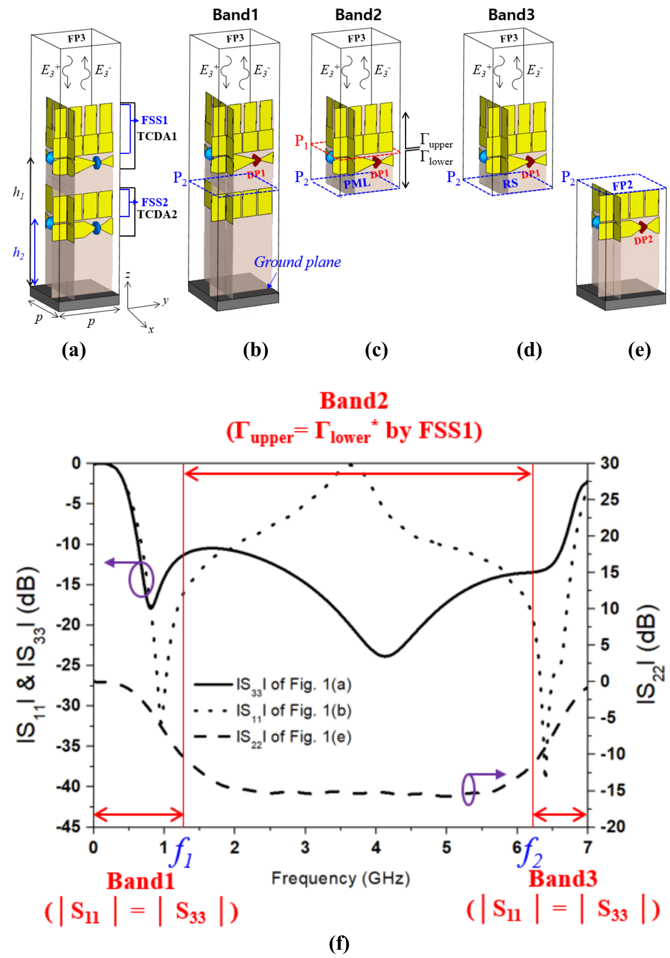

Fig. 1. Design of the proposed TCDA-under-TCDA absorber. E_3^+ and E_3^- are the incident and the reflected electric field at port 3, respectively. FP and DP indicate the Floquet port and discrete port (red cones), respectively. The port impedances of DP1, DP2, and FP are 240, 200, and 377 Ω, respectively. Resistances of lumped elements (blue cones) are 240 Ω for TCDA1 and 200 Ω for TCDA2. (a) TCDA-under-TCDA absorber. The equivalent structures of the TCDA-under-TCDA absorber at (b) band1, (c) band2, (d) band3, and (e) TCDA2 alone. (f) Reflection characteristics of the structure (a), (b), and (e). FP2 and DP2 have the same response of S_{22} by reciprocity. $S_{33} = E_3^-/E_3^+$.

The parameters of the equivalent circuits can be obtained as follows. The self-capacitances, C_2 and C_4 and the inductances of the dipole, L_2 and L_4 introduced in [27] are found by the parametric study. The coupling capacitances C_1 and C_3 can be obtained by extracting the odd mode capacitance by placing a PEC wall at the center of the gap between the two dipole arms. The self-inductances of the dipole, L_1 and L_3 can be found by the following equation [28]:

$$L_{1,3} = \frac{\mu_0 l_{1,3}}{4\pi} \ln \frac{2 l_{1,3}}{a_{e1,3}} \tag{1}$$

where $l_{1,3} = 2dw_{1,3}$ is the effective dipole length and $a_{e1,3} = 0.25 d_{h1,2}$ is the equivalent radius of a flat dipole [29]. $dw_{1,3}$ and $d_{h1,2}$ are denoted in Fig. 8(a); and μ_0 is the permeability of vacuum. The initial values of these four parameters are calculated and optimized to be fitted with a full-wave simulation of the TCDA without ground plane. Table I summarizes the values of the parameters of the final equivalent circuit.

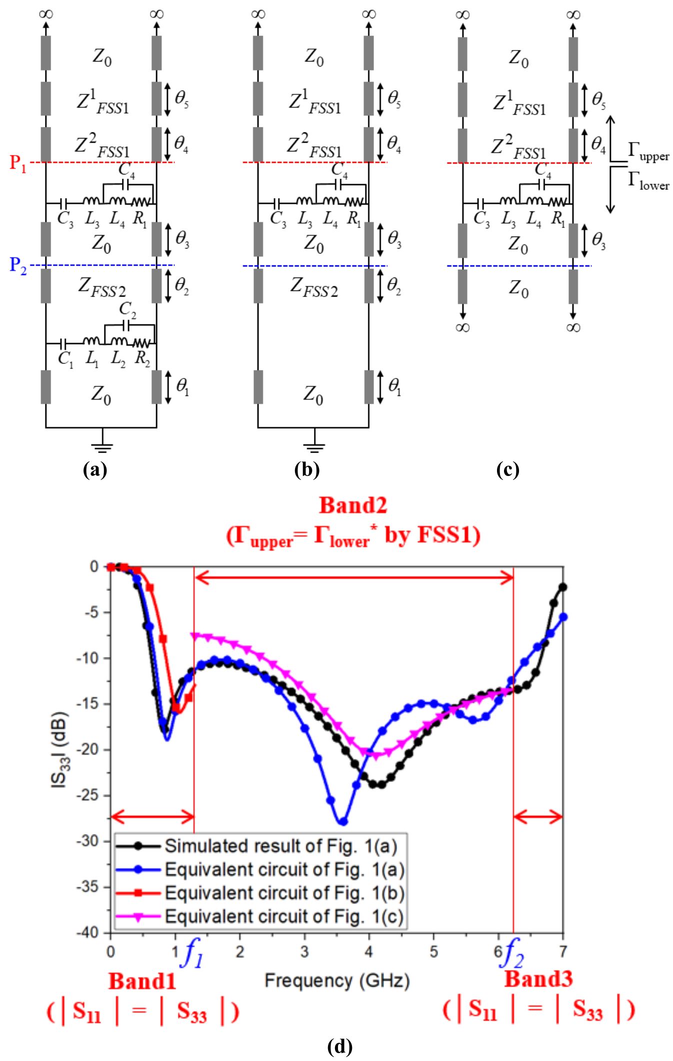

Fig. 2. Equivalent circuit of the proposed absorber shown in Fig. 1 (a) for whole band, (b) band1, and (c) band2. (d) Reflection characteristics, S_{33}, of each equivalent circuits compared with simulation results of proposed absorber structure.

TABLE I

VALUES OF THE PARAMETERS OF EQUIVALENT CIRCUIT: β_0 AND Z_0 ARE THE PROPAGATION AND CHARACTERISTIC IMPEDANCE IN FREE SPACE, RESPECTIVELY

L_1	C_1	L_2	C_2	L_3	C_3
6.238 nH	1.882 pF	2.687 nH	0.1753 pF	2.331 nH	0.503 pF
L_4	C_4	θ_1/β_0	$\theta_2/\beta_0/\sqrt{2.2}$	θ_3/β_0	$\theta_4/\beta_0/\sqrt{2.6}$
10.43 nH	0.046 pF	20 mm	8 mm	9 mm	6 mm
$\theta_5/\beta_0/\sqrt{1.2}$	Z^1_{FSS1}	Z^2_{FSS1}	Z_{FSS2}	R_1	R_2
9 mm	$Z_0/\sqrt{1.2}$	$Z_0/\sqrt{2.6}$	$Z_0/\sqrt{2.2}$	240 Ω	200 Ω

B. Design of the Proposed Absorber

Fig. 1(a) shows the basic structure of the proposed absorber unit cell. Before describing in detail the design steps for each structure, we summarize the unit cell design procedure as follows.

1) Design TCDA1 first as shown in Fig. 1(a) with a height of h_1. The lowest operating frequency of TCDA is roughly determined by $f_{lowest} \approx 0.09c/h$, where c and h are the speed of light and height of TCDA, respectively [8]. Hence, for TCDA1, $f_{1,lowest} \approx 0.09c/h_1$ and for TCDA2, $f_{2,lowest} = f_1 \approx 0.09c/h_2 = 2f_{1,lowest}$ since h_2 is designed to be $h_1/2$.
2) Design TCDA2 with a height of $h_1/2$ ($\approx h_2$) as shown in Fig. 1(e); it operates as an absorber by itself from f_1 to f_2 (band2). It can be designed for an approximate bandwidth of 5:1.
3) Insert TCDA2 into the empty space under TCDA1. TCDA2 can be designed to operate in the frequency range of f_1–f_2 ($f_2 \approx 5f_1$) so that the operating bandwidth of the whole absorber extends to $5f_1{:}f_1/2 \approx 10{:}1$.
4) Design the metasurface (MS) and vertical metal strip (VMS) for wide-angle insensitivity as shown in Fig. 6(a) (not shown in Fig. 1 for easy understanding of the basic structure of the proposed absorber unit cell).

1) Design of TCDA1 and Operation in Band1: TCDA1 is composed of the dipole and FSS1. The dipole of TCDA1 is designed with a p: h_1 ratio of 1:2 to operate at band1. Together with the two-layer impedance transformer, FSS1, which will be designed in step 3), a bandwidth of 0.67–2 GHz is obtained with a discrete port (DP) S_{11}, as shown by the dotted line in Fig. 1(f). In fact, in band1, although the dipole of TCDA2 with lumped resistor does not affect TCDA1 since the port of TCDA2 becomes almost open-circuited at a frequency lower than f_1 (band1) [15], FSS2 in Fig. 1(b) which is one of the low-impedance transmission lines has a little effect on TCDA1 and cannot be neglected. As a result, TCDA1, as designed above, operates as a near-lossless antenna at band1 even when TCDA2 is located under TCDA1, as in a TCDA-under-TCDA structure. Therefore, reciprocity can be applied to utilize TCDA1 as an absorber: $S_{33} = S_{11}$.

2) Design of TCDA2: In this study, the TCDA2 antenna is designed with the same ratio between the width and the height of the unit cell, p: $h_2 = 1 : 1$, such as in conventional TCDAs [30]. Since the radiation resistance of the absorber is 377 Ω at the FPs, it is difficult to transform this impedance to the low impedance of the antenna input port using a single-stage matching circuit. FSS1 and FSS2 are low-impedance transmission lines acting as impedance transformers in the equivalent circuit, by which the impedance matching circuit becomes a multistage matching circuit to widen the bandwidth. This results in an operating frequency range of 1.3(f_1)–6.22(f_2) GHz (band2) with DP 2, as shown by the dashed line in Fig. 1(e). Notice that TCDA2 is a near-lossless antenna and becomes a wideband absorber when it is in receiving mode [14]. In addition, it should be mentioned that TCDA2 results in a perfect matched layer (PML) boundary at P_2 in band2, and this fact is used to design the FSS1 of the TCDA1. Moreover, notice that the antenna impedance of TCDA2 is very reactive when the frequency is in band3.

3) Operation of TCDA1 in Band2: FSS1 should be carefully designed so that TCDA1 has absorber characteristics in band2. Since TCDA2 plays the role of a PML boundary at P_2 in band2, with respect to an antenna, CDA1 of the TCDA-under-TCDA is no longer a lossless antenna. Therefore,

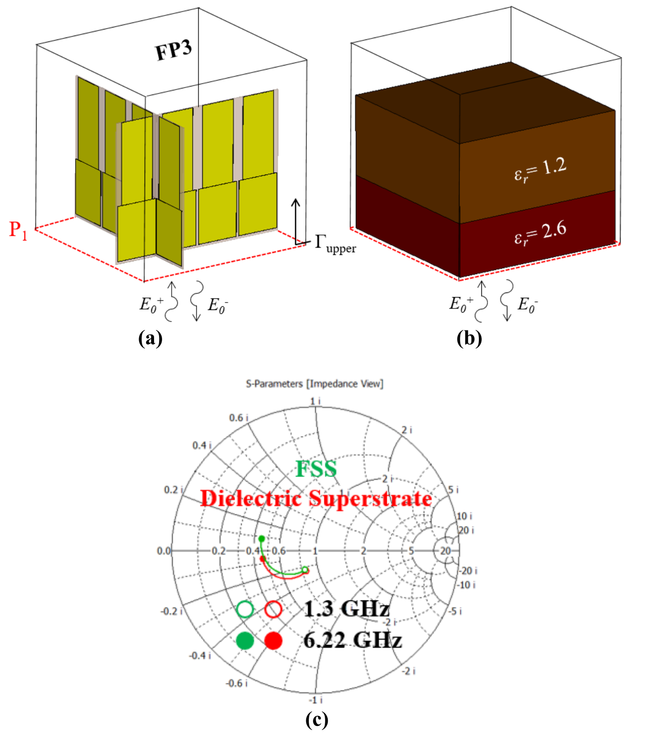

Fig. 3. Structure in periodic boundary and the comparison of the reflection coefficients (E_0^-/E_0^+). (a) FSS1. (b) Two-layer dielectric superstrate. Relative permittivity of each dielectric layer is 1.2 and 2.6. The length of these layers is the same. (c) Smith chart in band2 where it is normalized to free space impedance 377 Ω.

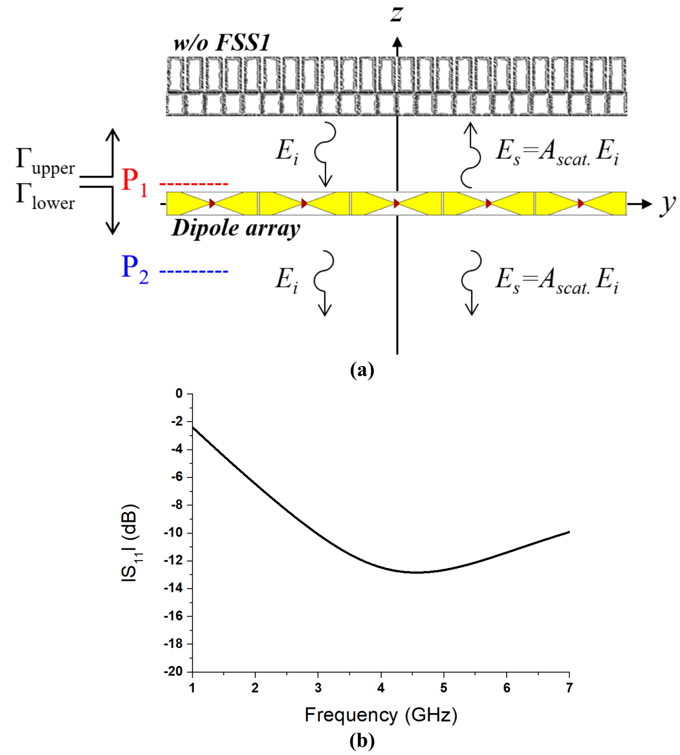

Fig. 4. (a) TCDA1 without FSS1: Geometry of an infinite dipole array in free-space excited by a plane wave where E_i and E_s are the incident and scattered electric fields, respectively. The dipole array extends infinitely far with period p in the x- and y-directions and has discrete port1 (red cones). (b) S_{11}.

we cannot apply the conventional approach of reciprocity to the design of an absorber from the design of a lossless antenna [14]. Considering that our goal is to match the input impedance of the FP 3 of the absorber looking from free-space in Fig. 1(a), we propose a method where the FP3 is matched by FSS1 after determining the reflection coefficient (Γ_{lower}) at P_1 in Fig. 1(c).

A multilayer dielectric superstrate shown in Fig. 3(b) can be a candidate for use as a wideband impedance transformer, where the dielectric constants of the layers are 1.2 and 2.6 [31]. It can be observed that the real part of the reflection coefficient (E_0^-/E_0^+) in Fig. 3(c) is negative; therefore, the impedance looking into the free space via the impedance transformer decreases over wide bands. However, a dielectric superstrate is large and expensive. In addition, it can generate surface waves, resulting in an undesirable situation [32]. Therefore, a light-weight and low-cost metal-based artificial superstrate (FSS) is introduced. Furthermore, this FFS does not generate surface waves [21]. The effective dielectric constant of the FSS is determined using the patch width and the gap between them. Using this principle, we designed the two-layer FSS1 in Fig. 3(a) and demonstrated the characteristic of reflection coefficients, as denoted by the green curve in Fig. 3(c). Considering that the thickness of each layer is the same as that of the two-layer dielectric superstrate and the characteristic of reflection coefficients is very similar over wide bands, the proposed FSS1 could be a suitable alternative.

For the equivalent structure shown in Fig. 1(c) at band2, to identify Γ_{lower} at P_1, we use the results obtained from a previous study [33], in which it was identified that a dipole array in free space can receive maximum power from the normal incident wave when the scattering coefficient (A_{scat}) is $-1/2$, as shown in Fig. 4(a), this phenomenon occurring when the input impedance of the dipole array antenna is perfectly matched. It should be noted that reference impedance of the reflection coefficient is the air impedance (=377 Ω) and the FSS1 should be ignored. Since the physical meaning of A_{scat} is that of the reflection coefficient by definition and the reference impedance of Γ_{lower} is the free space impedance, the reflection coefficient Γ_{lower} is equal to A_{scat}. Fig. 4(b) shows S_{11} of the TCDA1 without FSS1 (dipoles only) in free space. It indicates that the dipoles are well-matched in the frequency range of 1.3–6.22 (band2) except for the lower frequency part of band2. Consequently, Γ_{lower} is presumed to be approximately $-1/2$, thus the TCDA1 receives the maximum power from the normal incident wave in band2. Owing to this fact, for band2, we do not need to consider the complex equivalent circuit, such as that shown in Fig. 2(c).

Finally, if Γ_{upper} is equal to Γ_{lower}^*, S_{33}, in Fig. 1(c), will be 0 [34]. As mentioned before, the reflection coefficient (Γ_{lower}) between the perfectly matched dipole array antenna and free space is approximately $-1/2$, as shown in Fig. 5(a). In addition, because the imaginary part of Γ_{lower} is sufficiently small, its conjugation is not considerably different from Γ_{lower}. As a result, S_{33} becomes well-matched due to $\Gamma_{upper} \approx \Gamma_{lower}^*$ as shown in Fig. 5(b); therefore, our objective is attained for band2.

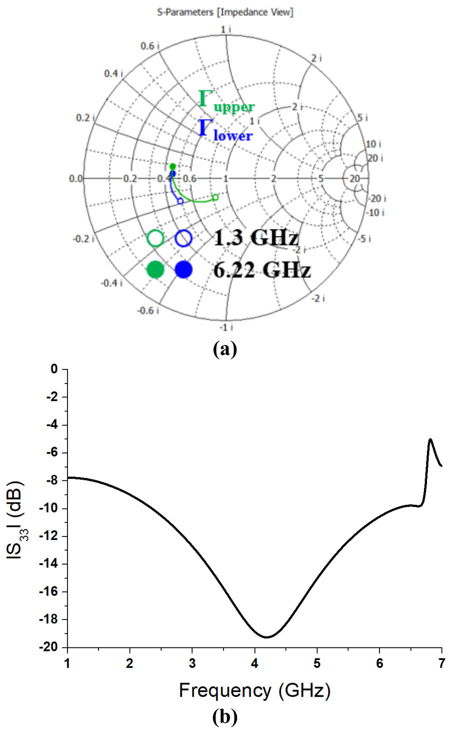

Fig. 5. (a) Γ_{upper} and Γ_{lower} are shown in a Smith chart where the results are normalized to free space impedance. (b) S_{33}.

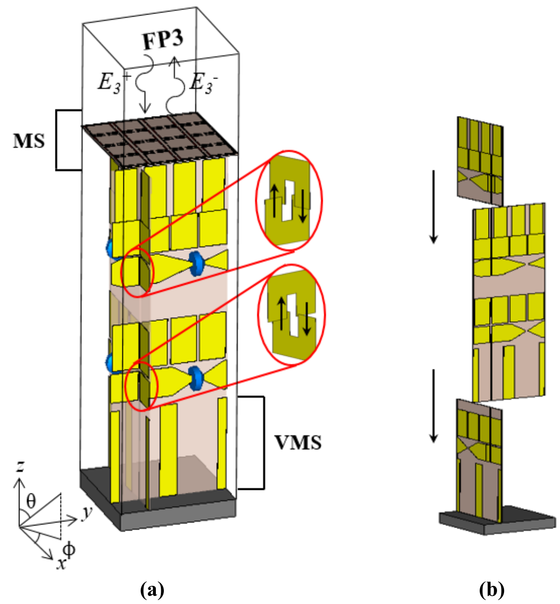

Fig. 6. (a) Proposed unit cell of the absorber based on the structure in Fig. 1(a) with added VMS and MS. Crossed overlapped patches in the back of the PCB are enlarged. (b) Structure of the orthogonal PCBs inserted into each other for the polarization insensitive absorber.

In band3, TCDA2 is in an OFF state again, thus it produces a high RS at P_2 and the downward wave from TCDA1 is minimally absorbed at TCDA2. As a result, TCDA1 in the TCDA-under-TCDA becomes a near-lossless antenna again, therefore reciprocity can be applied and the overall structure becomes an absorber.

4) Design of the MS and VMS: In existing studies on TCDAs, several approaches have been employed to realize wide-angle insensitivity for the TE mode [22] and TM mode [26]. In [22], a split ring resonator (SRR)-based MS was proposed, where the SRR exhibits a symmetric geometry in the E- and H-planes. The MS is composed of 4 × 4 SRRs and positioned at 2 mm above TCDA1, as shown in Fig. 6(a). In this study, the SRR patterns were modified into resistive SRR patterns using a resistive film [MS (film)] of 100 Ω/square (https://ohmega.com) since this film is more suitable than the pure imaginary series *LC* tanks of the nonresistive SRR [MS (copper)] at high-frequency bands, as confirmed in Fig. 7. In addition, Fig. 7 illustrates that the reflection coefficient (S_{33}) in the TE mode under a 45° oblique incidence is improved at 1–4 GHz by employing the MS (film).

For the TM mode, the decrease of the electrical length of h_2 at the oblique incidence angle significantly affects the impedance characteristic of the TCDA [26]. Nevertheless, it can be made insensitive by using a VMS, which makes the wavenumber move in the *z*-direction and wave impedance of the TM mode to be constant with the incidence angles [26]. As a result, the bandwidth can be extended from 0.99 to 6.26 GHz without VMS to 0.75 to 6.22 GHz with VMS, being thus widened by 32%, whereas the lowest operating frequency is decreased by 25%. It should be noted that the MS (film) and VMS do not significantly affect S_{33} under normal incidence. In addition, these operate independently so that the MS has little effect on the TM mode and vice versa. In summary, the bandwidth of 0.63–6.55 (10.4:1) for $S_{33} < -10$ dB is achieved with a $0.126\lambda_{\text{low}}$ at the lowest operating frequency under normal incidence. Furthermore, under 45° oblique incidence, the bandwidths of 0.69–6.75 (9.78:1) and 0.75–6.22 (8.29:1) are achieved with a $0.138\lambda_{\text{low}}$ and a $0.150\lambda_{\text{low}}$ for the TE mode and TM mode, respectively. By introducing the VMS and MS (film), the bandwidth and lowest operating frequencies for the TE and TM modes are almost constant with respect to the incidence angles. It should be noted that the bandwidth of the proposed structure under normal incidence is not so different from that of the structure without the VMS and MS (film).

For the absorption of the orthogonal polarization, a crossed TCDA-under-TCDA structure should be used [20]. Also, overlapped patches are employed to increase the mutual coupling between adjacent TCDAs, as shown in the enlarged photographs of Fig. 6(a). Since these are crossed, the patches are modified to a U-shape, whereas one of the two PCBs should be separated to join each other as shown in Fig. 6(b).

The actual geometrical dimensions of the proposed absorber unit cell are shown in Fig. 8 using FR-4 boards ($\varepsilon_r = 4.3$ and $\tan\delta = 0.025$) with a thickness of 0.2 mm.

Fig. 9 shows the S_{33} polarization dependence. Although the U-shaped patches are asymmetrical, the responses at different polarization angles are almost the same.

C. Discussion

In this work, the TCDA-under-TCDA structure has been proposed to increase the upper frequency of the absorber by five times without increasing the height of the original

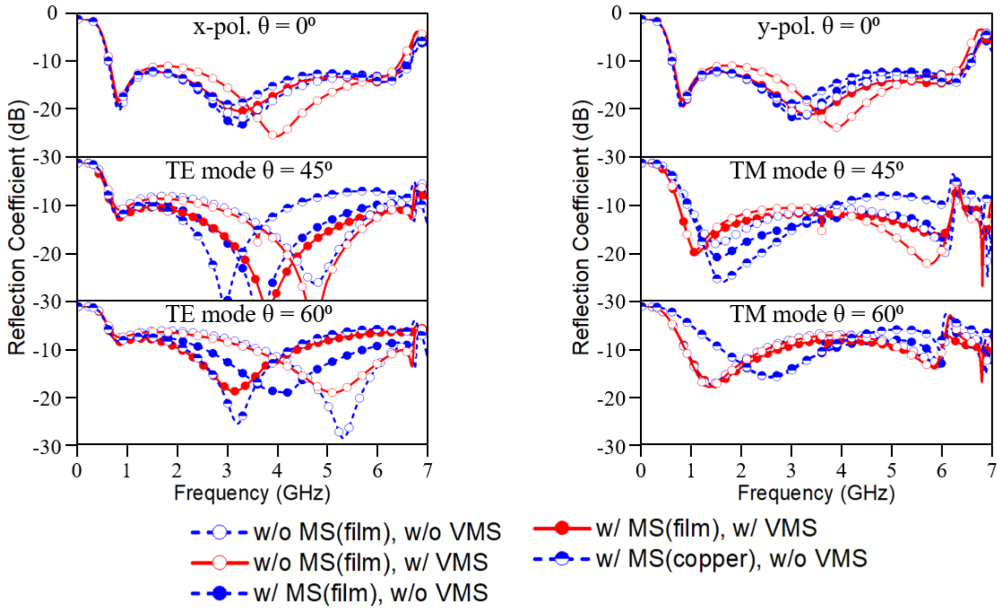

Fig. 7. Effects of VMS and MS on S_{33}. MS (film) and MS (copper) indicate the MS composed of a resistive film and copper, respectively. Without VMS and MS, the reflection coefficient is poor for an incident wave from 45° to 60°, especially in the low-frequency band. S_{33} becomes less than -10 dB up to 45° by introducing the VMS and MS (film). The results are independent of ϕ, as shown in Fig. 9.

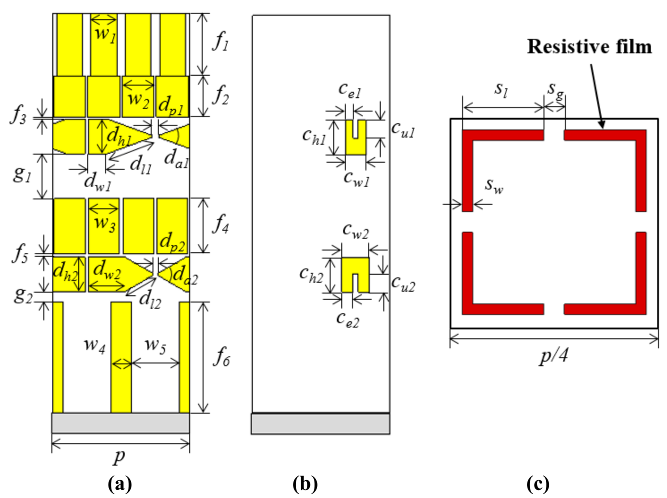

Fig. 8. Geometries of the proposed square unit cell. (a) Front ($w_1 = 3.8$ mm, $w_2 = 4.7$ mm, $w_3 = 4.5$ mm, $w_4 = 3$ mm, $w_5 = 7$ mm, $d_{p1} = 9$ mm, $f_1 = 9$ mm, $f_2 = 6$ mm, $f_3 = 0.3$ mm, $f_4 = 8$ mm, $f_5 = 0.5$ mm, $f_6 = 16$ mm, $g_1 = 6.5$ mm, $g_2 = 1.5$ mm, $d_{p1} = 0.5$ mm, $d_{h1} = 5$ mm, $d_{l1} = 6.88$ mm, $d_{a1} = 40°$, $d_{w1} = 2.83$ mm, $d_{p2} = 0.5$ mm, $d_{h2} = 5$ mm, $d_{l2} = 4.54$ mm, $d_{a2} = 60°$, $d_{w2} = 5.32$ mm, and $p = 20$ mm) and (b) back side of the TCDA-under-TCDA ($c_{e1} = 1.15$ mm, $c_{h1} = 5$ mm, $c_{u1} = 2.6$ mm, $c_{w1} = 3$ mm, $c_{e2} = 1.6$ mm, $c_{h2} = 5$ mm, $c_{u2} = 2.6$ mm, and $c_{w2} = 4$ mm). (c) Unit cell of the 4 × 4 square MS which is positioned at 2.2 mm on the top of the TCDA-under-TCDA. The red pattern is made of 100 Ω/square resistive film ($s_l = 2$ mm, $s_g = 0.5$ mm, and $s_w = 0.25$ mm). Total thickness of the unit cell including the MS is 60.2 mm.

TCDA1 absorber. This goal can be achieved by ingeniously placing a high-band TCDA2 into the empty space under the original TCDA1. The role of the VMS and MS is to help the TCDA-under-TCDA absorber to improve the TE mode reflection characteristics in the lower band at large incidence angles. To evaluate the contribution of each part to the performance of the proposed final structure, the Rozanov limit for the theoretical minimum thickness is considered [7]

$$d_{\min} \geq \frac{\left|\int_0^\infty \ln|\Gamma(\lambda)|\,d\lambda\right|}{2\pi^2} \approx \frac{\left|\int_{\lambda_{\min}}^{\lambda_{\max}} \ln|\Gamma(\lambda)|\,d\lambda\right|}{2\pi^2} \tag{2}$$

where $\Gamma(\lambda)$, λ_{max} and λ_{min} are the reflection coefficient of the absorber, the maximum, and minimum wavelengths corresponding to the claimed bandwidth for $|\Gamma(\lambda)| = -10$ dB, respectively. For TCDA1 only, the actual thickness-to-d_{min} ratio is 3.33. On the other hand, for TCDA-under-TCDA absorber without/with the VMS and MS, the actual thickness-to-d_{min} ratio is reduced to 2.28/2.32, respectively. As a result, it can be concluded that TCDA2 under TCDA1 does a key role to widen the bandwidth of the proposed absorber without the increase of the thickness of the original TCDA1 absorber structure.

III. Simulated and Experimental Results for the Proposed 1-D Absorber

To measure the backscattering coefficient (Γ) of the absorbers, a simple method with calibration has been employed [35], [36]: Only a 1-D sample is fabricated and measured using the TEM cell. A prototype of the proposed 1-D single-polarized absorber sample was fabricated and shown in Fig. 10(c). Fig. 10(a) and (b) shows the front and backside of the unit cell PCB, respectively. The lumped resistance elements of 200 and 240 Ω are realized using resistance chips (https://www.yageo.com). The PEC walls in Fig. 10(c) are attached to the sample to realize the stable boundary condition [37].

The TEM cell was designed to measure the 1-D sample, its geometry being shown in Fig. 11(a). The SMA connector (MC002126, http://www.multicomp-pro.com) was used for feeding the TEM cell at port1, whereas the other

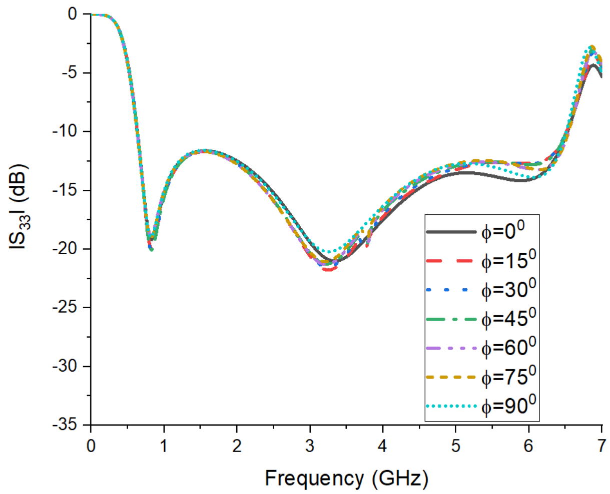

Fig. 9. S_{33} for normal incident wave with various polarization angles.

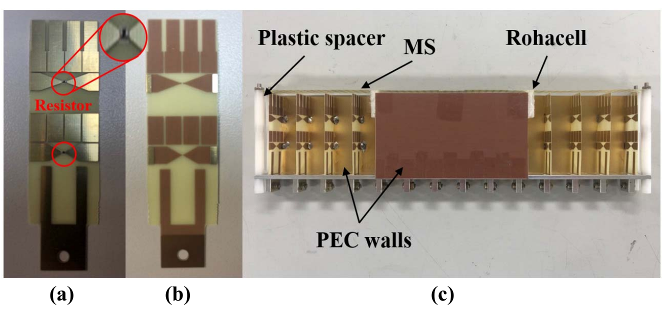

Fig. 10. (a) Front and (b) back of the unit cell PCB. The hole in the bottom helps joining the unit cell with the aluminum ground plane. (c) Prototype of 1 × 14 sample of the proposed absorber. Four plastic spacers and Rohacell foams support the MS. PEC walls are employed to make stable boundary condition.

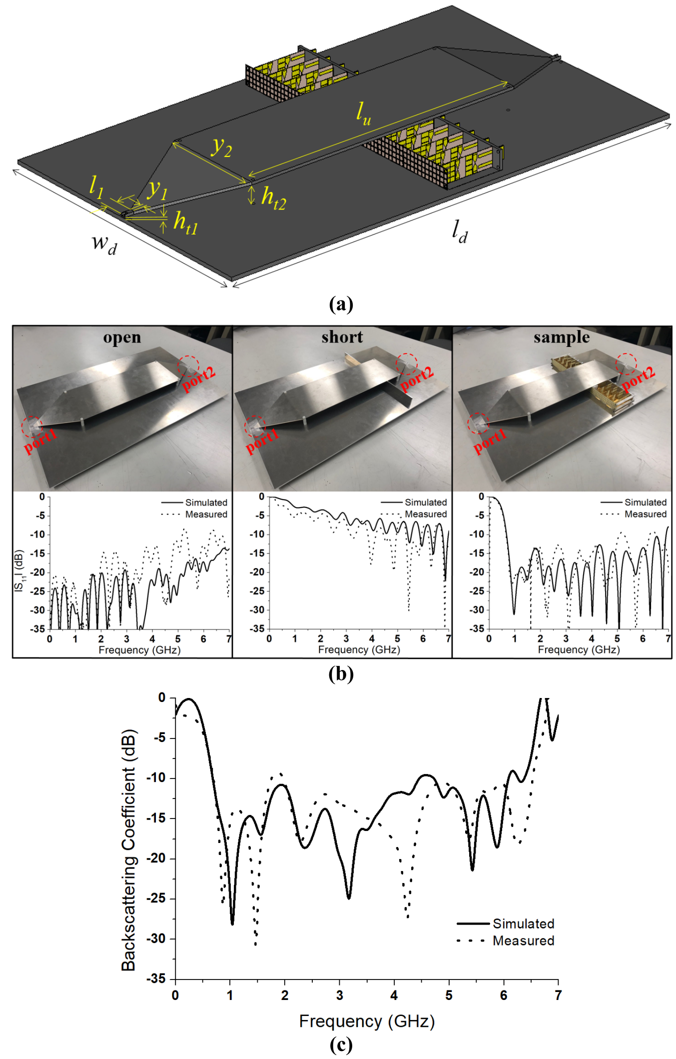

Fig. 11. Simulation, measurement setup, and results for the backscattering coefficient of the proposed absorber using TEM cell. (a) Perspective of the simulated TEM cell with 1-D absorber sample. $w_d = 300$ mm, $l_d = 500$ mm, $l_1 = 10$ mm, $y_1 = 4.7$ mm, $h_{t1} = 1$ mm, $y_2 = 108$ mm, $h_{t2} = 23.2$ mm, and $l_u = 300$ mm. (b) Simulated and measured S_{11} of the three cases with the port2 matched: open, short, and sample (left to right). (c) Simulated and measured backscattering coefficient.

port was matched-terminated. The width and thickness of the TEM cell should be designed such that the characteristic impedance of the TEM cell should be tapered for impedance matching so that only the TEM mode is excited. To identify Γ, S_{11} in three cases should be known: S_{11} without any structures in the TEM cell (Γ_{open}), S_{11} with the aluminum plate (Γ_{short}), and the sample (Γ_{sample}) in the TEM cell. In the calibration procedure, the inverse-Fourier transforms of the three parameters (Γ_{open}, Γ_{short}, and Γ_{sample}) and the time-gate of these parameters was implemented for reducing the multiple reflections. Finally, their Fourier transforms were implemented, and $\Gamma = (\Gamma'_{\text{sample}} - \Gamma'_{\text{open}})/(\Gamma'_{\text{short}} - \Gamma'_{\text{open}})$ was calculated, where the prime denotes the time-gated parameter. Fig. 11(b) and (c) shows the simulated and measured results of S_{11} for the three cases and the backscattering coefficient, respectively. The simulated bandwidth is 0.68–6.37 GHz (9.37:1) with a height of $0.136\lambda_{\text{low}}$ and the measured bandwidth is 0.69–6.53 GHz (9.46:1) with a height of $0.138\lambda_{\text{low}}$. These are in very good agreement with each other as well as with the unit cell simulation result shown in Fig. 7.

Table II shows a comparison of the proposed absorber's performances with those of state-of-the-art absorbers in terms of the thickness t, operating bandwidth, maximum oblique incidence angle θ_{max}, and figure of merit P_A normalized to t_{max}. The parameter, t, is the thickness of the absorber normalized to the wavelength at the lowest operating frequencies of each bandwidth for the TEM, TE, and TM modes when the oblique incidence angle changes from normal to maximum. t_{max} is the maximum value of t among all three bands. The figure of merit P_A normalized to t_{max} is defined as follows [38]:

$$NP_A = P_A/t_{\max} = \frac{B\log(1/|\Gamma_{\max}|)}{t_{\max}\cos\theta_{\max}} \tag{3}$$

where $B = (f_{\max} - f_{\min})/\sqrt{f_{\max} f_{\min}}$: f_{max} and f_{min} are the maximum and minimum operating frequencies within the common bandwidths of the TEM, TE, and TM modes from normal to maximum oblique incidence angles, respectively. $\Gamma_{\max}$ is the maximum reflection coefficient within that range. In all the previous absorbers, either the incidence angle is limited for wide bandwidth operation or the bandwidth is severely

TABLE II
COMPARISON OF SIMULATED RESULTS OF WIDEBAND AND LOW-PROFILE ABSORBERS

Work	Mode	t	Bandwidth	Incidence angle (°)	NP_A
[10]	TEM	0.076	3.67:1	0	8.49
	TE	**0.069***	**4.23:1***	30	
	TM	NG	NG	NG	
[11]	TEM	0.081	5.09:1	0	11.73
	TE	**0.087***	**4.47:1***	30	
	TM	**0.087***	**4.88:1***	30	
[12]	TEM	**0.15⁺**	**11.22:1⁺**	0	–
	TE	NG	NG	NG	
	TM	NG	NG	NG	
[13]	TEM	0.07	3.01:1	0	6.62
	TE	**0.069***	**3.05:1***	30	
	TM	0.079	2.61:1	30	
[16]	TEM	0.117	5.14:1	0	2.35
	TE	0.253	2.54:1	45	
	TM	0.232	3.05:1	45	
[17]	TEM	0.086	4.04:1	0	3.1
	TE	**0.093#**	**3.62:1#**	30	
	TM	0.108	2.64:1	30	
This work	TEM	0.126	10.4:1	0	14.21
	TE	0.138	9.78:1	45	
	TM	0.15	8.29:1	45	

NG: Not Given.
*Reference of backscattering coefficient is –7.7 dB.
+Reference of backscattering coefficient is –18.4 dB.
#Reference of backscattering coefficient is –9.4 dB.

deteriorated for wide incidence angle operation, particularly in the low-frequency band. In contrast, the proposed absorber shows ultra-wideband characteristics at the wide incidence angle of 45°. If a figure of merit normalized to t_{max} is used in order to take the absorber's thickness into account in addition to the bandwidth and maximum incidence angle for a fair comparison of the performances, the figure of merit of the proposed absorber is much higher than that of others, although the electrical height of the proposed absorber seems to be higher than others.

IV. CONCLUSION

In this article, an ultra-wideband and wide-angle insensitive absorber is proposed. The bandwidth can be extended by employing the TCDA-under-TCDA structure (2:1 × 5:1 = 10:1 bandwidth). In the frequency range where TCDA2 is in OFF-state, the conventional method using the reciprocity can be applied for the absorber's design. For the ON-state of the TCDA2 band, the impedance down-transformer (FSS1) can be used to match the impedance difference between P_1 and FP3; the reflection coefficient at boundary (P_1) between the dipole array and free space is $-1/2$. Finally, by introducing the MS and VMS, which are commonly used in TCDA antennas, the proposed absorber can be fabricated to be wide-angle insensitive to the TE and TM waves. It is worth noting that owing to our work, the antenna-based absorbers can be designed using both lossless and lossy antennas; this technique provides added flexibility in the design of antenna-based absorbers.

REFERENCES

[1] I. Bekkerman and J. Tabrikian, "Target detection and localization using MIMO radars and sonars," *IEEE Trans. Signal Process.*, vol. 54, no. 10, pp. 3873–3883, Oct. 2006.
[2] T.-H. Kim, H.-W. Jeon, J.-H. Shin, and Y.-D. Kang, "Improvement of detection ranges for targets in sidelobe clutter surroundings by sigma-delta STAP for airborne radars," *J. Electromagn. Eng. Sci.*, vol. 19, no. 4, pp. 234–238, Oct. 2019.
[3] J. Chen, Y. Shang, and C. Liao, "Double-layer circuit analog absorbers based on resistor-loaded square-loop arrays," *IEEE Antennas Wireless Propag. Lett.*, vol. 17, no. 4, pp. 591–595, Apr. 2018.
[4] X. Yuan *et al.*, "Wideband high-absorption electromagnetic absorber with chaos patterned surface," *IEEE Antennas Wireless Propag. Lett.*, vol. 18, no. 1, pp. 197–201, Jan. 2019.
[5] W. W. Salisbury, "Absorbent body for electromagnetic waves," U.S. Patent 2 599 944, Jun. 10, 1952.
[6] L. J. Du Toit, "The design of Jauman absorbers," *IEEE Antennas Propag. Mag.*, vol. 36, no. 6, pp. 17–25, Dec. 1994.
[7] K. N. Rozanov, "Ultimate thickness to bandwidth ratio of radar absorbers," *IEEE Trans. Antennas Propag.*, vol. 48, no. 8, pp. 1230–1234, Aug. 2000.
[8] B. A. Munk, *Frequency Selective Surfaces: Theory and Design*. Hoboken, NJ, USA: Wiley, 2005.
[9] G. Kim, S. Kim, and B. Lee, "Design of wideband microwave absorbers using reactive salisbury screens with maximum flat reflection," *J. Electromagn. Eng. Sci.*, vol. 19, no. 2, pp. 71–81, Apr. 2019.
[10] S. Ghosh, S. Bhattacharyya, and K. V. Srivastava, "Design, characterisation and fabrication of a broadband polarisation-insensitive multi-layer circuit analogue absorber," *IET Microw., Antennas Propag.*, vol. 10, no. 8, pp. 850–855, Jun. 2016.
[11] Z. Yao, S. Xiao, Z. Jiang, L. Yan, and B.-Z. Wang, "On the design of ultrawideband circuit analog absorber based on quasi-single-layer FSS," *IEEE Antennas Wireless Propag. Lett.*, vol. 19, no. 4, pp. 591–595, Apr. 2020.
[12] A. Kazemzade, "Nonmagnetic ultrawideband absorber with optimal thickness," *IEEE Trans. Antennas Propag.*, vol. 59, no. 1, pp. 135–140, Jan. 2011.
[13] N. Hakla, S. Ghosh, and K. V. Srivastava, "Design of low-profile broadband capacitive circuit absorber," *Electron. Lett.*, vol. 52, no. 22, pp. 1825–1826, Oct. 2016.
[14] X. Q. Lin, P. Mei, P. C. Zhang, Z. Z. D. Chen, and Y. Fan, "Development of a resistor-loaded ultrawideband absorber with antenna reciprocity," *IEEE Trans. Antennas Propag.*, vol. 64, no. 11, pp. 4910–4913, Nov. 2016.
[15] J. L. Volakis and K. Sertel, "Narrowband and wideband metamaterial antennas based on degenerate band edge and magnetic photonic crystals," *Proc. IEEE*, vol. 99, no. 10, pp. 1732–1745, Oct. 2011.
[16] C. Wu, S. Lu, Z. Yang, and Y. Yashchyshyn, "A UWB absorber based on the TCA concept in the UHF band," *IEEE Trans. Antennas Propag.*, vol. 68, no. 5, pp. 4132–4136, May 2020.
[17] F. Xu, S. Xiao, and Y. Li, "A broadband radiator and absorber based on tightly coupled array," in *Proc. 6th Asia–Pacific Conf. Antennas Propag. (APCAP)*, Oct. 2017, pp. 1–3.
[18] W. F. Moulder, K. Sertel, and J. L. Volakis, "Superstrate-enhanced ultrawideband tightly coupled array with resistive FSS," *IEEE Trans. Antennas Propag.*, vol. 60, no. 9, pp. 4166–4172, Sep. 2012.
[19] S. Kim and S. Nam, "Design of TCDA avoiding half-wavelength limitation using PC," in *Proc. 14th Eur. Conf. Antennas Propag. (EuCAP)*, Mar. 2020, pp. 1–4.
[20] J. P. Doane, K. Sertel, and J. L. Volakis, "A wideband, wide scanning tightly coupled dipole array with integrated balun (TCDA-IB)," *IEEE Trans. Antennas Propag.*, vol. 61, no. 9, pp. 4538–4548, Sep. 2013.
[21] E. Yetisir, N. Ghalichechian, and J. L. Volakis, "Ultrawideband array with 70° scanning using FSS superstrate," *IEEE Trans. Antennas Propag.*, vol. 64, no. 10, pp. 4256–4265, Oct. 2016.
[22] B. Wang, S. Yang, Y. Chen, S. Qu, and J. Hu, "Low cross-polarization ultrawideband tightly coupled balanced antipodal dipole array," *IEEE Trans. Antennas Propag.*, vol. 68, no. 6, pp. 4479–4488, Jun. 2020.
[23] O. Luukkonen, F. Costa, C. R. Simovski, A. Monorchio, and S. A. Tretyakov, "A thin electromagnetic absorber for wide incidence angles and both polarizations," *IEEE Trans. Antennas Propag.*, vol. 57, no. 10, pp. 3119–3125, Oct. 2009.

[24] S. Ghosh, S. Bhattacharyya, D. Chaurasiya, and K. V. Srivastava, "Polarisation-insensitive and wide-angle multi-layer metamaterial absorber with variable bandwidths," *Electron. Lett.*, vol. 51, no. 14, pp. 1050–1052, Jul. 2015.

[25] S. Chejarla, S. R. Thummaluru, and R. K. Chaudhary, "Flexible metamaterial absorber with wide incident angle insensitivity for conformal applications," *Electron. Lett.*, vol. 55, no. 3, pp. 133–134, Dec. 2019.

[26] S. Kim and S. Nam, "Bandwidth extension of dual-polarized 1-D TCDA antenna using VMS," *IEEE Trans. Antennas Propag.*, vol. 67, no. 8, pp. 5305–5312, Aug. 2019.

[27] E. A. Alwan, K. Sertel, and J. L. Volakis, "Circuit model based optimization of ultra-wideband arrays," in *Proc. IEEE Int. Symp. Antennas Propag.*, Jul. 2012, pp. 1–2.

[28] K. T. McDonald, "Reactance of small antennas," Joseph Henry Laboratories, Princeton Univ., Princeton, NJ, USA, Tech. Rep., 2012.

[29] C. A. Balanis, *Antenna Theory: Analysis and Design*. Hoboken, NJ, USA: Wiley, 2016.

[30] J. Zhong, A. Johnson, E. A. Alwan, and J. L. Volakis, "Dual-linear polarized phased array with 9:1 bandwidth and 60° scanning off broadside," *IEEE Trans. Antennas Propag.*, vol. 67, no. 3, pp. 1996–2001, Mar. 2019.

[31] B. A. Munk, *Finite Antenna Arrays and FSS*. Hoboken, NJ, USA: Wiley, 2003.

[32] W. H. Syed and A. Neto, "Front-to-back ratio enhancement of planar printed antennas by means of artificial dielectric layers," *IEEE Trans. Antennas Propag.*, vol. 61, no. 11, pp. 5408–5416, Nov. 2013.

[33] D.-H. Kwon and D. M. Pozar, "Optimal characteristics of an arbitrary receive antenna," *IEEE Trans. Antennas Propag.*, vol. 57, no. 12, pp. 3720–3727, Dec. 2009.

[34] D. M. Pozar, *Microwave Engineering*. Hoboken, NJ, USA: Wiley, 2009.

[35] T. Nakanishi, Y. Tamayama, and M. Kitano, "Efficient second harmonic generation in a metamaterial with two resonant modes coupled through two varactor diodes," *Appl. Phys. Lett.*, vol. 100, no. 4, Jan. 2012, Art. no. 044103.

[36] Y. Han and W. Che, "Low-profile broadband absorbers based on capacitive surfaces," *IEEE Antennas Wireless Propag. Lett.*, vol. 16, pp. 74–78, 2017.

[37] S. Kim and S. Nam, "Compact ultra-wideband antenna on folded ground plane," *IEEE Trans. Antennas Propag.*, vol. 68, no. 10, pp. 7179–7183, Mar. 2020.

[38] J. P. Doane, "Wideband low-profile antenna arrays: Fundamental limits and practical implementations," Ph.D dissertation, Ohio State Univ., Columbus, OH, USA, 2013.

Seongjung Kim received the B.S. degree in electronic and electrical engineering from Hongik University, Seoul, South Korea, in 2017. He is currently pursuing the integrated M.S. and Ph.D. degrees in electrical engineering and computer science with Seoul National University, Seoul.

His main research interests are metamaterial-based antennas and phased array antennas.

Sangwook Nam (Senior Member, IEEE) received the B.S. degree in electrical engineering from Seoul National University, Seoul, South Korea, in 1981, the M.S. degree in electrical engineering from the Korea Advanced Institute of Science and Technology (KAIST), Daejeon, South Korea, in 1983, and the Ph.D. degree in electrical engineering from The University of Texas at Austin, Austin, TX, USA, in 1989.

From 1983 to 1986, he was a Researcher with the Gold Star Central Research Laboratory, Seoul. Since 1990, he has been a Professor with the School of Electrical Engineering and Computer Science, Seoul National University. His research interests include the analysis/design of electromagnetic structures, antennas, and microwave active/passive circuits.